Quantum Monte Carlo studies of the ground states of heavy atoms in neutron-star magnetic fields

Steffen Bücheler, Dirk Engel, Jörg Main, and Günter Wunner*
Institut für Theoretische Physik 1, Universität Stuttgart, D-70550 Stuttgart, Germany
(Received 25 June 2007; published 10 September 2007)

The "released-phase" diffusion quantum Monte Carlo method is used to calculate the ground-state energies of atoms with nuclear charges from $Z=2,3,4,\ldots,26$ for magnetic field strengths relevant for neutron stars. The feature of our study is the use of adiabatic approximation wave functions as guiding wave functions to initialize the quantum Monte Carlo procedure. Our calculations are motivated by the discovery of broad features in the thermal spectra of isolated neutron stars, which may be due to heavy atoms. Our results confirm previous results for nuclear charge numbers up to 10, and are the most accurate ones available in the literature to date for $Z>10$.

DOI: 10.1103/PhysRevA.76.032501 PACS number(s): 31.25.Eb, 02.70.Uu, 32.60.+i, 71.10.−w

I. INTRODUCTION

The subject of atoms in strong magnetic fields has been a "hot topic" ever since the discovery of huge magnetic fields in white dwarf stars (10^3 to 10^5 T) and in neutron stars (10^6 to 10^9 T) in the 1970s. The intriguing new aspect of atomic physics at those field strengths is that the effects of the magnetic field become of the same order of, or larger than, the effects of the Coulomb binding, and thus nonperturbative, and atomic structure is completely rearranged. For the nth excited states of the simplest system, the hydrogen atom, the switchover from Coulomb field to magnetic field dominance occurs around B_0/n^3, with $B_0=4.701\,08\times10^5$ T the atomic unit of magnetic field strength, which shows that for low-lying states white dwarf magnetic fields are necessary, while for Rydberg states $n\sim30$ laboratory field strengths are sufficient to produce the nonperturbative, nonintegrable, situation which rendered the hydrogen atom in strong magnetic fields a paradigm of "quantum" chaos in the 1980s. A review of the relevant results for hydrogen and helium in strong magnetic fields, including their ramifications in astrophysics and chaos, up to 1994 can be found in Ref. [1].

A host of researchers, using a variety of methods, has since contributed to the field to make progress also for heavier atoms in magnetic fields. Among the methods were rigorous mathematical estimates [2–5], sparse grid combination techniques [6,7], density-functional calculations [8–13], finite-element methods [14–18], two-dimensional-discrete-variable methods on Laguerre meshes [19–21] or in combination with finite elements [22,23]. Different Hartree-Fock (HF) approaches were pursued: diagonalization in two-particle bases of Gaussian-type orbitals [24,25], HF calculations on finite-difference meshes [26–34], in adiabatic approximation with z-Slater-type orbitals [35–37], and finally HF calculations with r-Slater-type orbitals [38].

The discovery of the thermal emission spectra of isolated neutron stars with temperatures of a few 10^5 K, made possible by the launch of two x-ray satellites at the end of the 1990s, the Chandra X-Ray Observatory by NASA and the XMM-Newton Observatory by ESA, and the subsequent discovery of features in the x-ray spectra of the neutron star 1E 1207 [39] and three other isolated neutron stars [40–42] gave new impetus to studies of medium-Z elements in strong magnetic fields [43–45] since the observed features could be due to atomic transitions in elements that are fusion products of the progenitor star, and thus constituents of the thin atmospheric layer (with scale height $\sim0.1-10$ cm and density $\sim0.1-100$ g/cm^3 [46]) that covers the stellar surface. The elemental compositions of the atmospheres are presently not well known, and any element between H and Fe is feasible [44]. However, to calculate synthetic spectra for model atmospheres, and thus to be in a position to draw reliable conclusions from observed spectra to the elemental composition of the atmosphere and the distribution of elements on different ionization stages, accurate atomic data for these elements at very strong magnetic fields are indispensible.

In this paper we will apply a method to the problem of heavy atoms and ions in neutron star magnetic fields which, in principle, yields the exact ground state energies of interacting many-electron systems, namely, the *diffusion quantum Monte Carlo* method (DQMC). This method has been successfully employed in calculations of electronic ground state properties in solid state physics, but also in atomic and molecular physics. In particular, Ceperley and co-workers, the pioneers of the application of the DQMC method [47,48], in the 1990s also calculated energies of He in strong magnetic fields up to 10^5 T, where the Coulomb binding still dominates and an approach with guiding wave functions in spherical symmetry is viable.

It is the purpose of this paper to extend the DQMC method to neutron star magnetic field strengths $B\geq10^7$ T, where guiding wave functions must be used that account for the cylindrical symmetry imposed by the growing magnetic field dominance. To demonstrate the strength of the DQMC procedure we will apply it to the calculation of the ground state energies of many-electron atoms in strong fields with nuclear charges up to iron, $Z=26$, and compare with literature results wherever this is possible. We will also show that the application of the method to ions, which are of astrophysical interest, is straightforward.

The paper is organized as follows. Section II recapitulates the essential ingredients of the diffusion quantum Monte

*wunner@itp1.uni-stuttgart.de

Carlo method. The method is extended to the case of atoms at neutron star magnetic field strengths in Sec. III. There we propose to use adiabatic approximation Slater determinants, augmented by a Jastrow factor appropriate in magnetic fields, as guiding wave functions, and describe a way how to compute these efficiently. Finally, in Sec. IV, the method is demonstrated by applying it to the calculation of the ground state energies of neutral atoms and the ground state energies of iron ions in all ionization stages from heliumlike to neutral at neutron star magnetic field strengths.

II. DIFFUSION QUANTUM MONTE CARLO METHOD: ESSENTIALS

To render our presentation self-contained we briefly recapitulate the essential features of the DQMC method which will be necessary to understanding what follows. A detailed foundation of the method can be found in [47].

The basic idea is to identify the ground state wave function $\Phi_0(\vec{R},t)$ $[\vec{R}=(\vec{r}_1,\ldots,\vec{r}_n)]$ of an N-body Hamiltonian $\hat{H}$ with a *particle density* whose correct distribution is found by following the random walk of many test particles ("walkers") in imaginary time in $3N$-dimensional configuration space. The fact is exploited that in imaginary time evolution, $\tau=it$, any given initial distribution $\Psi(\vec{R},\tau)=\Sigma c_n\phi_n(\vec{R})e^{-(E_n-E_0)\tau}$, with $\phi_n(\vec{R})$ the stationary eigenfunctions of $\hat{H}$, will converge to the ground state ϕ_0 for $\tau\to\infty$, if E_0 is adjusted to be the true ground state energy. As is well known, in imaginary time the time-dependent Schrödinger equation turns into a diffusion equation for $\Psi(\vec{R},\tau)$, in which the total potential energy multiplied by the wave function takes the role of a source term. The Coulomb interactions between the charged particles cause large fluctuations at short ranges in simulations of the diffusion equation, which, however, can be greatly reduced by the technique of *importance sampling*.

The idea is to work with a probability distribution other than $\Psi(\vec{R},\tau)$ to obtain the same averages. To this end, the wave function is multiplied by a known trial function Ψ_G (guiding wave function), $f(\vec{R},\tau)\equiv\Psi(\vec{R},\tau)\Psi_G(\vec{R})$, which turns the Schrödinger equation in imaginary time for Ψ into a *drift-diffusion equation* for the density distribution $f(\vec{R},\tau)$,

$$-\frac{\partial f(\vec{R},\tau)}{\partial\tau}=\underbrace{-\frac{1}{2}\nabla^2 f}_{\text{diffusion}}+\underbrace{[E_L(\vec{R})-E_T]f}_{\text{branching}}+\underbrace{\nabla[f\vec{F_Q}(\vec{R})]}_{\text{drift}}. \tag{1}$$

In Eq. (1) the branching term is given by the "local excess energy" $E_L(\vec{R})-E_T$, where the "local energy" is defined by

$$E_L(\vec{R})=\hat{H}\Psi_G(\vec{R})/\Psi_G(\vec{R}), \tag{2}$$

and E_T is a trial energy offset which is adjusted during the simulation and eventually should converge to the correct ground state energy. The drift term contains the "quantum force" vector which depends on the guiding wave function,

$$\vec{F_Q}(\vec{R})\equiv\nabla\Psi_G(\vec{R})/\Psi_G(\vec{R}). \tag{3}$$

In a quantum Monte Carlo simulation, the drift-diffusion equation (1) describes both the propagation and the branching (i.e., creation or annihilation) of walkers.

To obtain the solution of (1), the equation is brought into integral form

$$f(\vec{R}',\tau+\Delta\tau)=\int d\vec{R}\tilde{G}(\vec{R}',\vec{R};\Delta\tau)f(\vec{R},\tau), \tag{4}$$

with the propagator

$$\tilde{G}(\vec{R}',\vec{R};\Delta\tau)=\langle\vec{R}'|e^{-\hat{H}\Delta\tau}|\vec{R}\rangle. \tag{5}$$

Since the kinetic and potential energy operators do not commute, a factorization of the time evolution operator (Trotter-Suzuki decomposition) is obtained only for small time steps,

$$\tilde{G}(\vec{R}',\vec{R};\Delta\tau)=\langle\vec{R}'|e^{-\hat{T}\Delta\tau}e^{-\hat{V}\Delta\tau}|\vec{R}\rangle+O(\Delta\tau^2), \tag{6}$$

where

$$\hat{T}=-\tfrac{1}{2}\vec{\nabla}^2+\vec{\nabla}\cdot\vec{F}(\vec{R}), \tag{7}$$

$$\hat{V}=[E_L(\vec{R})-E_T]. \tag{8}$$

Thus the propagator can be written in this "short-time approximation" as

$$\begin{aligned}\tilde{G}(\vec{R}',\vec{R};\Delta\tau)&\simeq e^{-\Delta\tau[E_L(\vec{R}')-E_T]}\langle\vec{R}'|e^{-\Delta\tau\hat{T}}|\vec{R}\rangle\\&=\tilde{G}_B(\vec{R}',\vec{R};\Delta\tau)\tilde{G}_D(\vec{R}',\vec{R};\Delta\tau),\end{aligned} \tag{9}$$

where the branching and diffusion (drift) Green's functions are given by

$$\tilde{G}_B(\vec{R}',\vec{R};\Delta\tau)=e^{-\Delta\tau[E_L(\vec{R}')-E_T]}, \tag{10}$$

$$\tilde{G}_D(\vec{R}',\vec{R};\Delta\tau)=\frac{1}{(2\pi\Delta\tau)^{3N/2}}e^{-[\vec{R}'-\vec{R}-\Delta\tau\vec{F}(\vec{R})]^2/2\Delta\tau}, \tag{11}$$

respectively. Whether a Monte Carlo move from $\vec{R}$ to $\vec{R}'$ in the time step $\Delta\tau$ is accepted or not is decided by the Metropolis algorithm [49],

$$P_{\text{accept}}(\vec{R},\vec{R}';\Delta\tau)=\min\left\{1,\frac{|\Psi_G(\vec{R}')|^2\tilde{G}_D(\vec{R},\vec{R}';\Delta\tau)}{|\Psi_G(\vec{R})|^2\tilde{G}_D(\vec{R}',\vec{R};\Delta\tau)}\right\}. \tag{12}$$

Since we have the condition $\Delta\tau\ll 1$ on the one hand and $\tau\to\infty$ on the other hand, it is evident that many time steps must be carried out in a simulation, which renders the simulation numerically expensive. The ground state energy in dynamical equilibrium is finally given by the arithmetic mean value of the local energies E_L evaluated at the positions of the walkers,

$$E_0=\langle E_L\rangle\equiv\lim_{\tau\to\infty}\frac{\int f(\vec{R},\tau)[\hat{H}\psi_G(\vec{R})/\psi_G(\vec{R})]d\vec{R}}{\int f(\vec{R},\tau)d\vec{R}}. \tag{13}$$

Because of its interpretation as a density distribution, $f(\vec{R},\tau)=\Psi(\vec{R},\tau)\Psi_G(\vec{R})$ must always be real and nonnegative. For $\Psi(\vec{R},\tau)$ and $\Psi_G(\vec{R})$ both real this implies that the nodes of the guiding wave function determine the nodes of the ground state, and both functions must change sign when crossing a nodal surface. Walkers which would lead to a change of sign in the density distribution are rejected. This is the "*fixed-node*" approximation (cf. [47,50]).

With the addition of a magnetic field the ground state will, in general, be complex valued. For complex-valued states the analogous method is the "*fixed-phase*" quantum Monte Carlo technique (FPDQMC) [51]. It assumes a trial phase of the complex many-body wave function, and exactly solves the resulting equation for its modulus using random walks. More specifically, both the state and the guiding wave function are decomposed into modulus and phase factor, and by defining $f(\vec{R},\tau)=\Psi^*(\vec{R},\tau)\Psi_G(\vec{R})$ the requirement that f be nonnegative is guaranteed by assuming the phases of state and guiding wave function to coincide. Dropping the imaginary part of the quantum force as part of the fixed-phase approximation, the quantum force is given by the real part of the logarithmic derivative of the guiding wave function

$$\vec{F}(\vec{R})=\frac{\vec{\nabla}|\Psi_G(\vec{R})|}{|\Psi_G(\vec{R})|}=\mathrm{Re}\left(\frac{\vec{\nabla}\Psi_G(\vec{R})}{\Psi_G(\vec{R})}\right). \tag{14}$$

By contrast, the local energy becomes complex valued, which implies that in the branching propagator,

$$\tilde{G}_B(\vec{R}',\vec{R};\Delta\tau)=e^{-\Delta\tau\{\mathrm{Re}[E_L(\vec{R}')]-E_T\}}\underbrace{e^{i\Delta\tau\,\mathrm{Im}[E_L(\vec{R}')]}}_{\varphi(\vec{R}',\Delta\tau)}, \tag{15}$$

the phase information $\varphi(\vec{R}',\Delta\tau)$ can be split off, and the simulation can still be performed in real space.

A final generalization is the "*released-phase*" method [52]: Every walker collects a total phase information of $\Upsilon(s)=\prod_{i=1}^{s}\varphi(i)$ during its random walk until step s, which contributes with its weight $\Upsilon(s)$ to the average of the local energy over all walkers. All final results in this paper have been obtained using the released-phase diffusion quantum Monte Carlo method (RPDQMC).

In Fig. 1 the structured flow of a RPDQMC simulation is shown. The essential steps are the following:

(1) initialize walkers distributed according to the guiding wave function $\Psi_G(\vec{R})$, determined in a forerunner variational MC which also yields the initial value for the trial energy E_T;

(2) move every walker $\vec{R}'=\vec{R}+\vec{\eta}+\Delta\tau\vec{F}_Q(\vec{R})$, where $\vec{\eta}$ is a Gaussian random vector with mean zero and standard deviation $\sqrt{\Delta\tau}$, and $\vec{F}_Q(\vec{R})$ is the local quantum force;

(3) accept move if Metropolis acceptance probability $P_{\mathrm{accept}}(\vec{R},\vec{R}';\Delta\tau)$ is greater than some random number $X\in[0,1]$;

(4) calculate the local energy $E_L(\vec{R}')$;

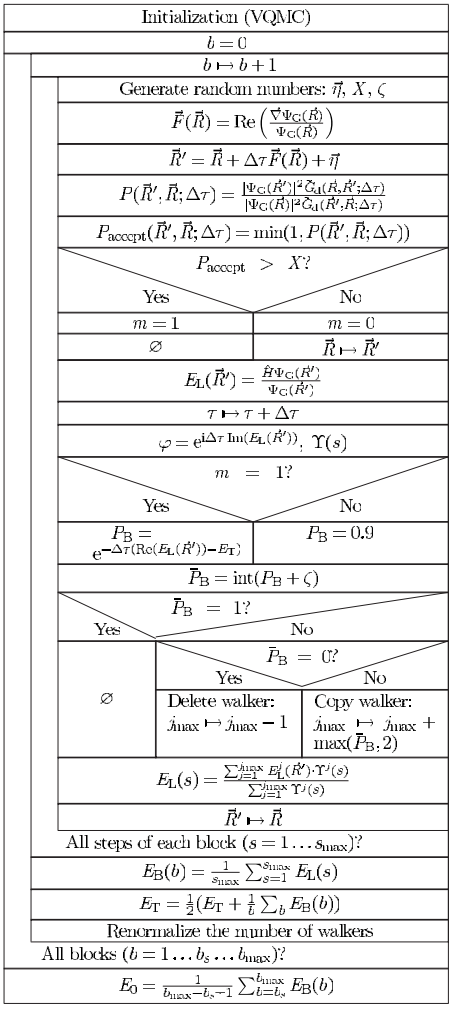

FIG. 1. Nassi-Shneiderman diagram of the released-phase DQMC method. The method is initialized by a variational quantum Monte Carlo simulation for the guiding wave function. The index b counts the number of calculations ("blocks"), in each block s steps are carried out, j is the walker index. In our simulations the total number of blocks was 700, the number of steps 200, and 500 walkers were used. The averaging over the block energies only starts at block b_s, where the walkers have reached dynamical equilibrium. The $m=1$ flag takes care of the rare cases where because of very low acceptance probabilities a walker becomes locked in some part of configuration space. Setting $P_B=0.9$ offers the possibility of either deleting or keeping this walker.

(5) release phase $\varphi(\vec{R}',\Delta\tau)$, determine accumulated phase $\Upsilon(s)$, execute branching according to the value of $P_B(\vec{R}')$, delete, keep, or copy walkers;

(6) average over local energies of all walkers in step s;

(7) loop over s until $s=s_{\max}$;

(8) average over s to obtain the block energy $E_B(b)$;

(9) update trial energy E_T;

(10) loop over blocks b until $b=b_{\max}$;

(11) average over blocks b to obtain the average block energy, and thus the final result for the ground state energy of the complete simulation.

III. DQMC FOR NEUTRON STAR MAGNETIC FIELD STRENGTHS

A. Choice of the guiding wave functions

The feature of our application of the diffusion quantum Monte Carlo method is the use of adiabatic approximation wave functions as guiding wave functions. That is, the guiding wave function of the N-electron atoms is taken to be a Slater determinant of single-particle orbitals ψ_i which are products of Landau states $\Phi_{n,m}$ and longitudinal wave functions $P_{n,m,\nu}$

$$\psi_i(\vec{r}) = \Phi_{nm}(\rho,\varphi)P_{nm\nu}(z). \tag{16}$$

Here n denotes the Landau level, m is the magnetic quantum number, and ν is the number of nodes of the longitudinal wave function. Since at neutron star magnetic field strengths the single-particle Coulomb excitation energies are much smaller than the spacing of the Landau levels, the cyclotron energy $\hbar\omega_B$ (≥ 1 keV for $B \geq 10^7$ T), it is sufficient to restrict oneself to the lowest Landau level $n=0$. In this level, all electrons have spin $s_z=-1/2$, and the spin quantum number can be omitted in what follows. While the Landau states are given by well-known analytical functions, the longitudinal wave functions must be determined numerically in a self-consistent way.

The intuitive meaning of the adiabatic approximation, introduced as early as 1937 by Schiff and Snyder [53], is that the magnetic field is strong enough that the "gyration" of the electron in the plane perpendicular to the magnetic field in quantized Landau orbits is "fast" compared with the oscillating motion of the electron in the direction of the field, which is caused by the Coulomb attraction of the positively charged nucleus or core. For this motion the electron effectively "sees" only the Coulomb attraction averaged over the Landau state.

Defining the reference magnetic field B_Z where for a nuclear charge Z the switchover from Coulomb to magnetic field dominance occurs by $B_Z=Z^2B_0 \approx Z^2 4.701\times 10^5$ T, and introducing the dimensionless magnetic field parameter $\beta_Z = B/B_Z$, one can write the condition for the adiabatic approximation to hold quantitatively as $\beta_Z \geq 1$. For $\beta_Z=1$ the Larmor radius $a_L=\sqrt{2\hbar/eB}$ becomes equal to the effective Bohr radius $a_Z=a_0/Z$ for nuclear charge Z, and the cyclotron energy is 4 times the effective Rydberg energy $E_Z=Z^2E_{\mathrm{Ryd}}$ (a_0 and E_{Ryd} are the Bohr radius and Rydberg energy of the hydrogen atom, respectively).

A stumbling block in the construction of the Slater determinant of the N-electron atom in an intense magnetic field is that no clear shell structure exists as in the field-free case. An inspection of the energy level spectrum of the single-electron problem shows (see, e.g., Fig. 9.1 in Ruder *et al.* [1]) that the states are ordered in tightly bound states, whose energies monotonously increase with decreasing magnetic quantum number $m=0,-1,-2,\ldots$, and hydrogenlike states with an energy spectrum roughly corresponding to that of s states of the field-free hydrogen atom. The natural choice is to place the electrons successively into the tightly bound magnetic sublevels until degeneracy with hydrogenlike states occurs, and hydrogenlike states with low absolute values of the magnetic quantum number must be populated.

Hartree-Fock calculations for many-electron atoms in adiabatic approximation were first performed by Neuhauser *et al.* [35] and later by Miller and Neuhauser [36]. Our approach [54] differs from theirs in that we employ more advanced and efficient numerical techniques, viz. finite elements and B-spline interpolation [55,56]. More specifically, the interval $[0,z_{\max}]$ on the z axis is divided into n finite elements $I_j=[z_{j-1},z_j]$ with quadratically widening element borders $[z_k=k^2z_{\max}/n^2,\ k=0,1,\ldots,n]$, and the longitudinal part of each single-particle orbital $\psi_i(\vec{r}) \equiv \Phi_i(\rho,\varphi)P_i(z)$ is expanded in terms of B splines, $P_i(z)=\Sigma_l \alpha_l^{(i)} B_l(z)$. The advantage of using B splines, as opposed to Lagrange or Hermite interpolation, lies in their global definition on the interval $[0,z_{\max}]$. The expansion coefficients $\alpha_l^{(i)}$ are determined by converting the energy extremum principle into an equivalent one for the coefficients, and numerically solving the resulting system of inhomogeneous linear equations

$$\sum_{j,l} A_{kl}^{(j)} \alpha_l^{(i)} = -\sum_j b_k^{(j)}. \tag{17}$$

The matrix $A_{kl}^{(j)}$ and the vector $b_k^{(j)}$ for single-particle orbital ψ_i are given by

$$A_{kl}^{(j)} = \int_{I_j} dz B_k(z)\hat{A}B_l(z), \tag{18}$$

$$b_k^{(j)} = \int_{I_j} dz B_k(z)b(z), \tag{19}$$

where the integration extends over the jth finite element I_j, and

$$\hat{A} = \frac{\partial^2}{\partial z^2} - V_i^{\mathrm{EF}}(z) + \epsilon_i - \sum_{\substack{j=1 \\ j\neq i}}^{N} \int_{-\infty}^{\infty} dz' P_j^2(z') W_{ij}^{\mathrm{DI}}(z,z'), \tag{20}$$

$$b(z) = \sum_{\substack{j=1 \\ i\neq j}}^{N} P_j(z) \int_{-\infty}^{\infty} dz' P_j(z') P_i(z') W_{ij}^{\mathrm{EX}}(z,z'). \tag{21}$$

In Eq. (20), $V_i^{\mathrm{EF}}(z)$ is the expectation value of the nuclear potential with respect to the Landau orbital Φ_i and ϵ_i is a Lagrange parameter, and in (21) $W_{ij}^{\mathrm{DI}}(z,z')$ and $W_{ij}^{\mathrm{EX}}(z,z')$ denote the direct and exchange potential terms of the electron-electron interaction with respect to the Landau orbitals Φ_i and Φ_j. Since the potentials depend on the longitudinal wave functions, and thus on the coefficients, the solution must be found iteratively in a self-consistent way. The iteration is initialized by distributing the electrons on magnetic sublevels according to the level scheme of the hydrogen atom in intense magnetic fields and by appropriate core charge scaling of the z-dependent wave functions. In our calculations, we used sixth-order B splines and typically 15 finite elements. The maximum integration radius $z_{\max}$ was

chosen such that all longitudinal wave functions have decayed exponentially ($z_{\max} \sim 2-5$ atomic units). A more detailed description of the method along with results for energies and oscillator strengths in adiabatic approximation, calculated with it, will be presented elsewhere [57].

In the DQMC simulation, the evaluation of the quantum force requires the derivative of the adiabatic approximation guiding wave function. This can be accomplished in a straightforward way. The derivative of a Slater determinant with respect to a particle coordinate is again a Slater determinant, which in one column includes derivatives of the single-particle orbitals. The derivatives of the Landau functions with respect to the ρ and φ coordinates can be calculated analytically, and the derivatives of the B-spline basis functions with respect to z are particularly simple because of their form and their polynomial nature. This clearly is a big advantage of our ansatz.

B. Jastrow factors

The pure Slater-determinant form of the guiding wave function Ψ_G^{ad} so far does not include correlation effects among the electrons and with the nucleus. To incorporate such effects it is common to introduce a Jastrow factor, i.e., to define a new guiding wave function $\Psi_G = \Psi^{\mathrm{JF}} \Psi_G^{\mathrm{ad}} = e^{-U(|\vec{r}|)} \Psi_G^{\mathrm{ad}}$, where the Jastrow factor Ψ^{JF} is to modify the guiding wave function at small distances, but to converge to a constant value at large distances. For the electron-electron (EE) and electron-nucleus (EN) correlations $U = u_{\mathrm{EE}} + u_{\mathrm{EN}}$ we adopt the forms

$$u_{\mathrm{EE}} = \sum_{\substack{i,j=1 \\ i<j}}^{N} \frac{a_{\mathrm{EE}}^{\mathrm{JF}} r_{ij}}{1 + b_{\mathrm{EE}}^{\mathrm{JF}} r_{ij}}, \quad r_{ij} = |\vec{r}_i - \vec{r}_j|, \tag{22}$$

$$u_{\mathrm{EN}} = \sum_{i=1}^{N} \frac{a_{\mathrm{EN}}^{\mathrm{JF}} r_i}{1 + b_{\mathrm{EN}}^{\mathrm{JF}} r_i}, \quad r_i = |\vec{r}_i|. \tag{23}$$

For a specific choice of a^{JF} the Jastrow factor Ψ^{JF} removes the Coulomb singularity ("cusp condition" for vanishing electron-nucleus or electron-electron distance [58]). The inverse length parameters $b_{\mathrm{EE}}^{\mathrm{JF}}$ and $b_{\mathrm{EN}}^{\mathrm{JF}}$ can be used to optimize the guiding wave function. For simplicity, here we choose both parameters equal, $b_{\mathrm{EE}}^{\mathrm{JF}} = b_{\mathrm{EN}}^{\mathrm{JF}} \equiv b^{\mathrm{JF}}$. Our Jastrow factor for an N-electron atom in a strong magnetic field thus reads

$$\Psi^{\mathrm{JF}} = \exp\left(\frac{1}{4} \sum_{\substack{i,j=1 \\ i<j}}^{N} \frac{r_{ij}}{1 + b^{\mathrm{JF}} r_{ij}} - Z \sum_{i=1}^{N} \frac{r_i}{1 + b^{\mathrm{JF}} r_i} \right). \tag{24}$$

Figure 2 shows the expectation value of the energy of the ground state E_{VQMC} of neon in a magnetic field of $B = 10^8$ T with respect to $\Psi_G = \Psi^{\mathrm{JF}} \Psi_G^{\mathrm{ad}}$ as a function of the Jastrow parameter b^{JF}. The energy value is evaluated by performing a QMC simulation with $|\Psi_G|^2$ as distribution function. The energy value in adiabatic approximation (upper horizontal line at −10.4 keV) and the final result of the RPDQMC simulation (lower horizontal line) are shown for comparison, as is the standard deviation σ of the local energy. It is evident that there exists an optimum value of $b^{\mathrm{JF}} \approx 14.58$, which already lowers the adiabatic approximation energy by approximately two-thirds of its distance to the released-phase value. It can also be seen that close to the optimum value the standard deviation also becomes minimum. We note that the optimum value of b^{JF} lies close to $\sqrt{\beta}$. This is not unexpected since the characteristic inverse length in a magnetic field is the inverse of the Larmor radius, which, in atomic units, is $1/(a_L/a_o) = \sqrt{\beta}$. Therefore in all calculations we fixed $b^{\mathrm{JF}} = \sqrt{\beta}$. It follows that the Jastrow factor effectively modifies the adiabatic approximation guiding wave function only at distances smaller than the Larmor radius.

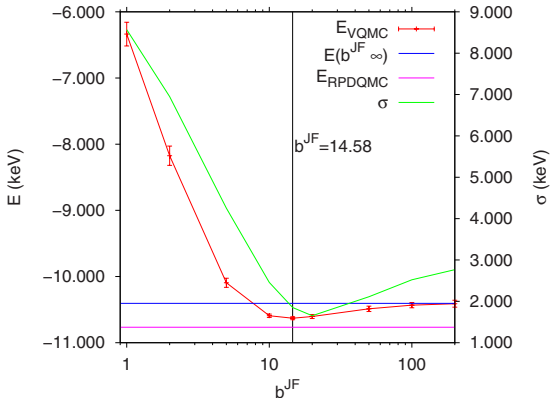

FIG. 2. (Color online) Ground state energy E_{VQMC} and the standard deviation σ of the local energy in dependence of the Jastrow parameter b^{JF} for neon ($Z=10$) and $B=10^8$ T. $E(b^{\mathrm{JF}} \to \infty)$ (upper horizontal line) corresponds to the case where no Jastrow factor is present, i.e., to the energy value in adiabatic approximation. E_{RPDQMC} (lower horizontal line) is the final result of the released-phase simulation.

The inclusion of the Jastrow factor leads, via the product rule, to additional terms in the derivatives of the guiding wave function, and thus in the quantum force. These, however, can again be treated analytically. We note that the Jastrow factor does not so much influence the final RPDQMC energy values but rather reduces the fluctuations of the block energies and leads to acceptance probabilities of greater than 99%, which are signatures of good QMC simulations.

IV. RESULTS AND DISCUSSION

To speed up the results, we parallelized the DQMC simulation code. The parallelization strategy, which exploited the message passing interface commands *reduce* and *broadcast*, was (a) distribute walkers on the available nodes, which independently run the DQMC procedure for the number of steps given, (b) after each block, calculate the block average values collecting the information from all nodes via *reduce*, adjust the trial energy E_{T}, *broadcast* it to all nodes, (c) for load balancing, after branching redistribute the walkers on the nodes via *broadcast*.

Our calculations were performed on the cacau cluster of the High Performance Computing Center Stuttgart (HLRS), where we used 25 double-processor nodes (3.2 GHz,

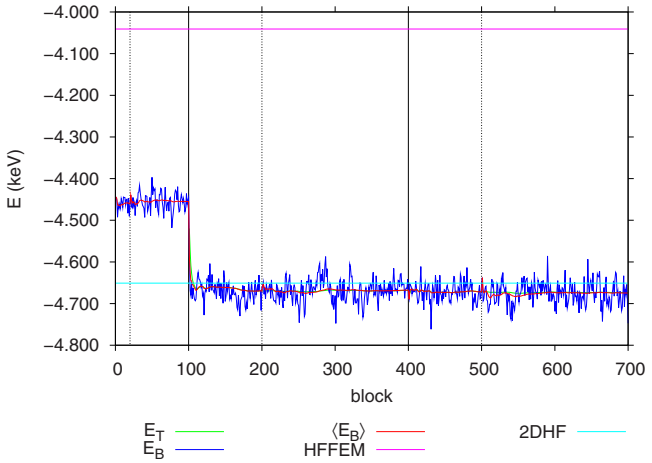

FIG. 3. (Color online) Behavior of the block energy E_B (ragged curve) and the averaged block energy $\langle E_B \rangle$ (smooth curve) in the DQMC simulation for the ground state energy of neon ($Z=10$) at $B=10^7$ T as a function of the number of blocks. The simulation is divided in three stages, indicated by the black vertical lines: a VQMC, a FPDQMC, and a RPDQMC simulation. The value at the end of the simulation is $E_0=-4.675$ keV. The dashed vertical lines indicate the blocks where dynamical equilibrium of the walkers is reached. In each block, 200 time steps $\Delta\tau=10^{-4}$ a.u. were performed. [HFFEM (top horizontal line), energy value in adiabatic approximation; 2DHF (bottom horizontal line), energy value of Ivanov and Schmelcher [29].]

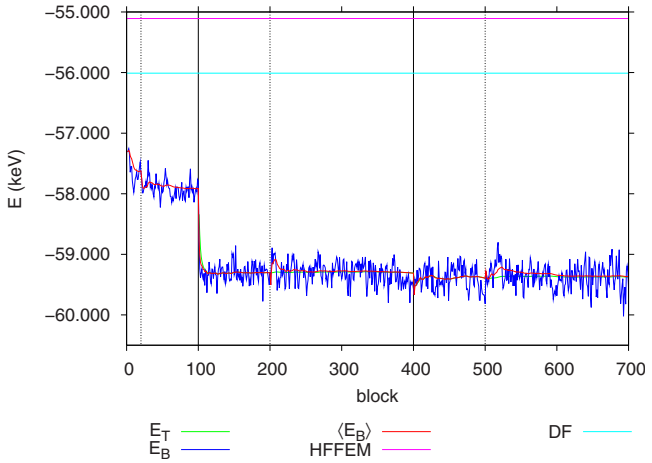

FIG. 4. (Color online) Same as Fig. 3, but for the ground state energy of iron ($Z=26$) at $B=10^8$ T. The value at the end of the simulation is $E_0=-59.366$ keV. Here in each block 200 time steps $\Delta\tau=2\times10^{-5}$ a.u. were performed. [HFFEM (top horizontal line), energy value in adiabatic approximation; DF (second horizontal line from top), density-functional result of Jones [9].]

1 GByte RAM per node). The advantage of parallelization is evident from the fact that, e.g., the run time of the calculation of the ground state of iron (26 electrons) at $B=10^8$ T could be reduced from 223 hours on a single-processor machine to 4.5 hours. This highlights the importance of the availability of parallel high performance computers for this type of simulation.

For the ground state of neon at $B=10^7$ T, Fig. 3 shows the typical flow of a diffusion quantum Monte Carlo simulation. The figure depicts the energy offset E_T, the block energy E_B, and the averaged block energy $\langle E_B \rangle$ as a function of the number of blocks performed. For comparison, the energy value in the adiabatic approximation determined with our own Hartree-Fock finite-element calculation (HFFEM) and the hitherto best energy value obtained by a two-dimensional Hartree-Fock method (2DHF) [29] are shown as horizontal lines. The complete simulation goes through three stages. During the first 100 blocks, a variational quantum Monte Carlo calculation is performed. Since the adiabatic approximation guiding wave function is augmented by the Jastrow factor, the VQMC calculation already lowers the energy in comparison with the initial adiabatic approximation result. This stage is followed, in the next 300 blocks, by a fixed-phase diffusion quantum Monte Carlo simulation. It is seen that the onset of the simulation leads to a considerable drop in the energy. Finally, in the last 300 blocks a released-phase

TABLE I. Energy values in keV for the ground states from helium to neon at $B=10^7$ T. (RPDQMC, released-phase; FPDQMC, fixed-phase; VQMC, variational quantum Monte Carlo simulation; HFFEM, Hartree-Fock finite-element method in adiabatic approximation; 2DHF, two-dimensional Hartree-Fock [29]; MCPH^3, multiconfigurational perturbative hybrid Hartree-Hartree-Fock [43]. Numbers in parentheses at the HFFEM results designate the number of electrons occupying an excited state. Parameters of the QMC simulations, 500 walkers; time step $\Delta\tau=10^{-4}$ a.u.)

Z	RPDQMC	FPDQMC	VQMC	HFFEM	2DHF	MCPH^3
2	−0.2649	−0.2649	−0.2617	−0.2556	−0.26387	−0.2613
3	−0.5421	−0.5422	−0.5329	−0.5167	−0.54042	−0.5337
4	−0.9029	−0.9020	−0.8845	−0.8474	−0.89833	−0.8897
5	−1.338	−1.338	−1.305	−1.239	−1.33229	−1.327
6	−1.847	−1.849	−1.792	−1.687	−1.83895	−1.854
7	−2.432	−2.429	−2.349	−2.184	−2.41607	
8	−3.100	−3.093	−2.980	−2.752(1)	−3.08253(1)	
9	−3.846	−3.841	−3.686	−3.373(1)	−3.82966(1)	
10	−4.675	−4.668	−4.455	−4.041(1)	−4.65087(1)	

TABLE II. Energy values in keV for the ground states from helium to silicon at $B=5\times10^7$ T. (Designations and parameters as in Table I.)

Z	RPDQMC	FPDQMC	VQMC	HFFEM	2DHF	MCPH[3]
2	−0.4626	−0.4629	−0.4592	−0.4551	−0.46063	−0.4567
3	−0.9661	−0.9653	−0.9575	−0.9459	−0.96180	−0.9526
4	−1.622	−1.621	−1.606	−1.582	−1.61624	−1.600
5	−2.421	−2.418	−2.393	−2.349	−2.41101	−2.390
6	−3.349	−3.345	−3.306	−3.236	−3.33639	−3.308
7	−4.402	−4.398	−4.344	−4.234	−4.38483	−4.353
8	−5.573	−5.564	−5.491	−5.336	−5.55032	−5.517
9	−6.857	−6.849	−6.749	−6.535	−6.82794	−6.803
10	−8.250	−8.242	−8.100	−7.826	−8.21365	−8.198
11	−9.752	−9.740	−9.572	−9.205		−9.718
12	−11.400	−11.392	−11.116	−10.729 (1)		−11.410 (1)
13	−13.163	−13.148	−12.877	−12.331 (1)		−13.251 (1)
14	−15.031	−15.013	−14.672	−14.020 (2)		−15.246 (2)

TABLE III. Energy values in keV for the ground states from helium to iron at $B=10^8$ T. Parameters of the QMC simulations, 500 walkers; time steps $\Delta\tau(Z=2,\ldots,10)=10^{-4}$ a.u., $\Delta\tau(Z=11,\ldots,19)=5\times10^{-5}$ a.u., $\Delta\tau(Z=20,\ldots,26)=2\times10^{-5}$ a.u. (DF, density-functional results).

Z	RPDQMC	FPDQMC	VQMC	HFFEM	2DHF	MCPH[3]	DF
2	−0.5827	−0.5827	−0.5791	−0.5754	−0.57999	−0.5766	−0.6035[a]
3	−1.230	−1.229	−1.220	−1.211	−1.22443	−1.214	
4	−2.081	−2.080	−2.065	−2.044	−2.07309	−2.056	
5	−3.122	−3.119	−3.095	−3.057	−3.10924	−3.085	
6	−4.338	−4.331	−4.294	−4.236	−4.31991	−4.288	−4.341[a]
7	−5.716	−5.712	−5.660	−5.568	−5.69465	−5.657	
8	−7.252	−7.246	−7.173	−7.045	−7.22492	−7.176	
9	−8.938	−8.930	−8.834	−8.658	−8.90360	−8.845	
10	−10.766	−10.753	−10.630	−10.400	−10.72452	−10.664	−10.70[b]
11	−12.725	−12.716	−12.569	−12.266		−12.625	
12	−14.827	−14.817	−14.618	−14.249		−14.745	
13	−17.061	−17.043	−16.813	−16.352 (1)		−16.973 (1)	
14	−19.480	−19.461	−19.185	−18.619 (1)		−19.408 (1)	−19.09[b]
15	−22.022	−22.009	−21.665	−21.002 (1)		−21.987 (1)	
16	−24.700	−24.668	−24.275	−23.482 (2)		−24.718 (2)	
17	−27.541	−27.523	−27.044	−26.130 (2)		−27.618 (2)	
18	−30.529	−30.509	−29.950	−28.890 (2)		−30.766 (2)	
19	−33.650	−33.605	−32.999	−31.756 (2)		−34.036 (2)	
20	−36.891	−36.881	−36.145	−34.750 (3)		−37.500 (3)	−35.48[b]
21	−40.296	−40.274	−39.458	−37.865 (3)			
22	−43.867	−43.821	−42.900	−41.083 (3)			
23	−47.526	−47.490	−46.458	−44.426 (4)			
24	−51.360	−51.271	−50.102	−47.877 (4)			
25	−55.279	−55.224	−53.915	−51.430 (5)			
26	−59.366	−59.311	−57.913	−55.108 (5)			−56.01[b]

[a]Medin and Lai [13].
[b]Jones [9].

TABLE IV. Energy values in keV for the ground states from helium to iron at $B=5\times10^8$ T. Parameters of the QMC simulations: 500 walkers; time steps $\Delta\tau(Z=2,\ldots,22)=10^{-5}$ a.u., $\Delta\tau(Z=23,\ldots,26)=5\times10^{-6}$ a.u.

Z	RPDQMC	FPDQMC	VQMC	HFFEM	2DHF	MCPH[3]	DF
2	−0.9664	−0.9672	−0.9620	0.9589	−0.96191	−0.9574	−1.04[a]
							−1.05[b]
3	−2.103	−2.101	−2.088	−2.080	−2.08931	−2.078	
4	−3.630	−3.626	−3.607	−3.591	−3.61033	−3.586	
5	−5.525	−5.524	−5.491	−5.465	−5.49950	−5.476	
6	−7.766	−7.764	−7.727	−7.679	−7.73528	−7.695	−8.03[a]
							−8.04[b]
7	−10.343	−10.336	−10.279	−10.214	−10.29919	−10.231	
8	−13.224	−13.221	−13.144	−13.055	−13.17543	−13.099	
9	−16.412	−16.407	−16.314	−16.185	−16.34997	−16.264	
10	−19.881	−19.873	−19.738	−19.594	−19.81072	−19.702	−20.24[a]
							−20.44[b]
11	−23.635	−23.614	−23.489	−23.268		−23.406	
12	−27.655	−27.629	−27.446	−27.199		−27.436	
13	−31.931	−31.888	−31.696	−31.376		−31.675	
14	−36.442	−36.421	−36.192	−35.793		−36.154	−36.76[a]
15	−41.203	−41.179	−40.898	−40.438		−40.915	
16	−46.214	−46.173	−45.852	−45.308		−45.881	
17	−51.445	−51.407	−51.030	−50.395		−51.067	
18	−56.894	−56.856	−56.425	−55.693		−56.530	
19	−62.584	−62.532	−62.044	−61.196		−62.181	
20	−68.447	−68.414	−67.934	−66.901		−68.031	−68.37[a]
21	−74.669	−74.605	−73.989	−72.899(1)		−74.184(1)	
22	−81.071	−81.039	−80.358	−79.112(1)		−80.602(1)	
23	−87.633	−87.652	−86.876	−85.530(1)		−87.263(1)	
24	−94.561	−94.494	−93.667	−92.148(1)		−94.259(1)	
25	−101.615	−101.549	−100.590	−98.964(1)		−101.25 (1)	
26	−109.079	−108.966	−107.913	−106.134(2)		−108.64(2)	−108.18(2)[a]
							−107.20(2)[c]

[a]Jones [9].
[b]Braun [12].
[c]Medin and Lai [13].

diffusion quantum Monte Carlo simulation is carried out, which still slightly lowers the averaged block energy, by roughly 0.1%. The relatively small difference between the fixed-phase and the released-phase results indicates that the phase of the adiabatic approximation wave function already well reproduces the phase of the ground state wave function. The small fluctuations of the individual block energies E_B evident in Fig. 3 are a typical feature of diffusion quantum Monte Carlo simulations. However, it is also seen that the averaged block energies $\langle E_B\rangle$ quickly converge to constant values in all three stages of the simulation. Our final RPDQMC result for the averaged block energy is $E_0=-4.675$ keV and lies slightly below the 2DHF value. The mean square deviation of the individual block energies from the average, which accounts for their fluctuations, at the end of the calculation is found to be $\sigma=\pm0.024$ keV, and thus encompasses the 2DHF value.

It should be noted, however, that the statistical error bar measures only the uncertainty in the measured quantity. This statistical uncertainty (standard deviation) is inversely proportional to the square of the number of independent averages, and thus may be reduced by making more or larger computer runs. Previous applications of the DQMC scheme [47,50] have shown that the absolute errors can in fact be much smaller.

For the much heavier element iron ($Z=26$) and the higher field strength of $B=10^8$ T the behavior of the simulation as a function of the number of blocks performed is shown in Fig. 4. The lowest energy value available in the literature so far was obtained in a density-functional calculation [9] and is shown for comparison by the horizontal line marked by DF. The behavior in the three stages, variational, fixed phase, released phase, is very similar to that observed in Fig. 3. Our final RPDQMC result for the energy is $E_0=-59.366$ keV and

lies well below the DF value. The standard deviation of the block energies at the end of the simulation in this case is $\sigma = \pm 0.132$ keV.

In Tables I–IV, the results of our diffusion Monte Carlo simulations for the ground state energies of medium-Z atoms at different magnetic field strengths are summarized. Each table contains in the first three columns the results of the three stages of the simulation (released phase, fixed phase, variational) and in the fourth column the energy values in the adiabatic approximation calculated with our own Hartree-Fock finite-element method. Literature values obtained by Ivanov and Schmelcher [29] (2DHF), by Mori and Hailey [43] (MCPH^3, multiconfigurational perturbative hybrid Hartree-Hartree-Fock), and the results of density-functional calculations by Jones [9], Braun [12], and Medin and Lai [13] (DF) are given in the remaining columns. The numbers in parentheses attached to the HFFEM, 2DHF, MCPH^3, and DF results designate the number of electrons occupying an excited hydrogenlike single-particle longitudinal state.

Table I shows the results for the ground state energies for the elements from helium to neon at $B=10^7$ T, Table II shows the results for the elements from helium to silicon at $B=5\times10^7$ T, and Tables III and IV list the results for all elements from helium to iron at the magnetic field strengths $B=10^8$ T, $B=5\times10^8$ T, respectively. For the maximum nuclear charge numbers in each table the β_Z values still are of the order of 1, or slightly less ($\beta_{Z=10}=0.21$ in Table I, $\beta_{Z=14}=0.54$ in Table II, $\beta_{Z=26}=0.31$ in Table III, $\beta_{Z=26}=1.57$ in Table IV). Note that even though at these values the adiabatic approximation becomes poor, as is evident from the HFFEM energies given in the tables, the adiabatic approximation wave function itself still can serve as a useful guiding wave function, since the final distribution of walkers has distinctly moved away from it.

The tables reveal that already the fixed-phase results lie slightly below the values that were obtained using the 2DHF method. The comparison with the results of the MCPH^3 method shows that our RPDQMC energy values generally lie below those results, but there are also exceptions where our results lie above the MCPH^3 energies. This may be due to the fact that the hybrid method is not self-consistent, since, first, it evaluates the exchange energy in first-order perturbation theory in a basis of Hartree states, and, second, it does not include the back-reaction of the excited Landau states whose admixtures are taken into account perturbatively on the effective interaction potentials. Therefore the method need not necessarily produce an upper bound on the energy.

The comparison with the results of the DF calculations shows that these yield lower ground state energies at small nuclear charge numbers than our RPDQMC results, while for large Z the reverse is the case. It must be remembered, however, that there are various proposals as to which form of the exchange energy functional should be chosen in the presence of a strong magnetic field. The DF results listed in Tables III and IV differ in the choice of the exchange functional. Given this restriction, it cannot be ensured that the DF calculations in all cases produce an upper bound on the ground state energy in magnetic fields as do the *ab initio* methods used in this paper and by Ivanov and Schmelcher [29].

The method presented in this paper can easily be extended to the calculation of the ground state energies of ions in neutron star magnetic fields. The prerequisite for initializing the DQMC procedure is again determining the adiabatic approximation guiding wave function for the respective ion. Thus the main task is to find appropriate initial longitudinal wave functions for performing the HFFEM calculation. Sample results for the ground state energies of iron ions in all ionization stages from heliumlike to neutral for a magnetic field strength of 5×10^8 Tesla are given in Table V. In this case, the simulations were carried out on a PC, and only 10 blocks were used for the VQMC and 100 blocks each for the fixed-phase and released-phase calculation, respectively. The improvement of the adiabatic approximation energy values by the DQMC simulations is clearly evident from Table V. In one instance ($n=23$) the fixed-phase result is seen to lie slightly below the released-phase result. This is a consequence of the lower block numbers used and indicates that the numbers given in Table V are accurate to within four significant figures. Clearly, this accuracy can again be improved by more extended calculations. It must be noted, however, that for charged many-particle systems in magnetic fields the generalized momentum is no longer conserved (cf.

TABLE V. Ground state energies in keV for iron in all ionization stages from heliumlike to neutral at $B=5\times10^8$ T. Numbers in parentheses at the HFFEM results: number of electrons occupying an excited state. Parameters of the QMC simulations, 500 walkers; time step $\Delta\tau=8\times10^{-6}$ a.u., only 210 blocks were used.

Number e^-	HFFEM	RPDQMC	FPDQMC	VQMC
2	−32.163	−34.503	−34.495	−33.781
3	−41.738	−44.267	−44.223	−43.453
4	−49.668	−52.315	−52.225	−51.634
5	−56.460	−59.141	−59.076	−58.319
6	−62.393	−65.079	−65.003	−64.197
7	−67.636	−70.362	−70.304	−69.620
8	−72.306	−75.047	−74.984	−74.097
9	−76.486	−79.250	−79.195	−78.488
10	−80.239	−82.992	−82.944	−82.049
11	−83.614	−86.375	−86.338	−85.552
12	−86.782(1)	−89.550	−89.484	−88.627
13	−89.633(1)	−92.401	−92.331	−91.341
14	−92.182(1)	−94.979	−94.845	−94.029
15	−94.454(1)	−97.238	−97.201	−96.331
16	−96.472(1)	−99.260	−99.201	−98.125
17	−98.254(1)	−101.06	−100.92	−100.07
18	−99.817(1)	−102.64	−102.51	−101.56
19	−101.17(1)	−104.00	−103.89	−102.82
20	−102.36(2)	−105.12	−105.05	−103.98
21	−103.39(2)	−106.19	−106.07	−105.16
22	−104.24(2)	−107.08	−107.00	−105.96
23	−104.93(2)	−107.70	−107.73	−106.56
24	−105.47(2)	−108.26	−108.23	−106.96
25	−105.87(2)	−108.70	−108.66	−107.37
26	−106.13(2)	−109.08	−108.97	−107.91

[1]), and energy corrections arise from the gyration of the ion as a whole in the magnetic field (cf. [59]). A comprehensive compilation of the ground state energies of different ions at neutron star magnetic field strengths will be the subject of a future presentation.

The RPDQMC energy values listed in Tables I–V represent the most comprehensive and accurate compilation for the ground state energies of medium-Z atoms up to iron in neutron star magnetic field strengths calculated by an *ab initio* method to date.

V. CONCLUSIONS

We have extended the released-phase diffusion Monte Carlo method to neutron star magnetic field strengths by using adiabatic approximation wave functions as guiding wave functions. We have thus been able to determine the ground state energies of neutral atoms from helium to iron in the range 10^7 to 5×10^8 T. No previous application of the released-phase method to atoms in strong magnetic fields has succeeded in coping with such large electron numbers. We have also shown that the method can be equally applied to the calculation of the ground state energies of ions at such magnetic field strengths. We have not considered relativistic effects, which are expected to be on the order of $(Z\alpha)^2$, and the effects of the finite nucleus mass. These effects are small compared with the observational uncertainties of spectral features and the smearing of spectral lines by the variation of the magnetic field across the neutron star's atmosphere. However, for matching observed thermal spectra from isolated neutron stars, wavelength information, and thus energies of excited states, are requisite. Jones *et al.* [52] have shown a way how to calculate excited states of small atoms in strong magnetic fields using the correlation function Monte Carlo method [48]. It will be an intriguing task to transfer their method to the DQMC simulations presented in this paper, and to calculate excited states of large atoms in intense fields.

ACKNOWLEDGMENTS

The authors thank Erik Koch for helpful discussions at an early stage of these investigations and Matthias Klews for providing his version of the HFFEM code. The authors also thank Alen Prskalo for running the HFFEM and DQMC codes for iron ions. This work was supported by Deutsche Forschungsgemeinschaft within the SFB 382 "Methods and algorithms for simulating physical processes on high-performance computers" at the Universities of Tübingen and Stuttgart.

[1] H. Ruder, G. Wunner, H. Herold, and F. Geyer, *Atoms in Strong Magnetic Fields* (Springer, Heidelberg, 1994).
[2] E. H. Lieb, J. P. Solovej, and J. Yngvason, Phys. Rev. Lett. **69**, 749 (1992).
[3] E. H. Lieb, J. P. Solovej, and J. Yngvason, Commun. Pure Appl. Math. **47**, 513 (1994).
[4] E. H. Lieb, J. P. Solovej, and J. Yngvason, Commun. Math. Phys. **16**, 77 (1994).
[5] E. H. Lieb, J. P. Solovej, and J. Yngvason, in *The Stability of Matter: From Atoms to Stars, Selecta of E. H. Lieb*, edited by W. Thirring (Springer, Heidelberg, 1997), pp. 145–167.
[6] S. Hilgenfeldt, S. Balder, and C. Zenger, Technische Universität München, Technical Report No. SFB 342/05/95, 1995 (unpublished).
[7] J. Garcke and M. Griebel, J. Comput. Phys. **165**, 694 (2000).
[8] L. Fritsche, Phys. Rev. B **33**, 3976 (1986).
[9] P. B. Jones, Mon. Not. R. Astron. Soc. **216**, 503 (1985).
[10] D. Kössl, R. G. Wolff, E. Müller, and W. Hillebrandt, Astron. Astrophys. **205**, 347 (1988).
[11] B. M. Relovsky and H. Ruder, Phys. Rev. A **53**, 4068 (1996).
[12] M. Braun, Phys. Rev. A **65**, 033415 (2002).
[13] Z. Medin and D. Lai, Phys. Rev. A **74**, 062507 (2006).
[14] J. Ackermann, B. Erdmann, and R. Roitzsch, J. Chem. Phys. **101**, 7643 (1994).
[15] J. Ackermann and J. Shertzer, Phys. Rev. A **54**, 365 (1996).
[16] M. Braun, W. Schweizer, and H. Elster, Phys. Rev. A **57**, 3739 (1998).
[17] L. R. Ram-Mohanans, S. Saigal, D. Dossa, and J. Shertzer, Comput. Phys. **4**, 50 (1990).
[18] J. Shertzer and F. S. Levin, Phys. Rev. A **43**, 2531 (1991).
[19] J. C. Light, I. P. Hamilton, and J. V. Lill, J. Chem. Phys. **82**, 1400 (1985).
[20] D. Baye and P.-H. Heenen, J. Phys. A **19**, 2041 (1986).
[21] D. Baye and M. Vincke, J. Phys. B **24**, 3531 (1991).
[22] V. S. Melezhik, Phys. Rev. A **48**, 4528 (1993).
[23] W. Schweizer and P. Faßbinder, Comput. Phys. **11**, 641 (1997).
[24] W. Becken, P. Schmelcher, and F. K. Diakonos, J. Phys. B **32**, 1557 (1999).
[25] S. Jordan, P. Schmelcher, W. Becken, and W. Schweizer, Astron. Astrophys. **335**, L33 (1998).
[26] M. V. Ivanov, J. Phys. B **27**, 4513 (1998).
[27] M. V. Ivanov and P. Schmelcher, Phys. Rev. A **57**, 3793 (1998).
[28] M. V. Ivanov and P. Schmelcher, Phys. Rev. A **60**, 3558 (1999).
[29] M. V. Ivanov and P. Schmelcher, Phys. Rev. A **61**, 022505 (2000).
[30] M. V. Ivanov and P. Schmelcher, J. Phys. B **34**, 2031 (2001).
[31] O. A. Al-Hujaj and P. Schmelcher, Phys. Rev. A **67**, 023403 (2003).
[32] O. A. Al-Hujaj and P. Schmelcher, Phys. Rev. A **68**, 053403 (2003).
[33] O. A. Al-Hujaj and P. Schmelcher, Phys. Rev. A **70**, 033411 (2004).
[34] O. A. Al-Hujaj and P. Schmelcher, Phys. Rev. A **70**, 023411 (2004).
[35] D. Neuhauser, K. Langanke, and S. E. Koonin, Phys. Rev. A **33**, 2084 (1986).
[36] M. C. Miller and D. Neuhauser, Mon. Not. R. Astron. Soc.

253, 107 (1991).
[37] M. Rajagopal, R. W. Romani, and M. C. Miller, Astrophys. J. **479**, 347 (1997).
[38] M. D. Jones, G. Ortiz, and D. M. Ceperley, Phys. Rev. A **54**, 219 (1996).
[39] S. Mereghetti, A. de Luca, P. A. Caraveo, W. Becker, R. Mignami, and G. F. Bignami, Astrophys. J. **581**, 1280 (2002).
[40] F. Haberl, A. D. Schwope, V. Habaryan, G. Hasinger, and C. Motch, Astron. Astrophys. **403**, L19 (2003).
[41] F. Haberl, V. E. Zavlin, J. Trümper, and V. Burwitz, Astron. Astrophys. **419**, 1077 (2004).
[42] M. H. van Kerkwijk, D. L. Kaplan, D. L. Durant, S. R. Kulkarni, and F. Paerels, Astrophys. J. **608**, 432 (2004).
[43] K. Mori and C. J. Hailey, Astrophys. J. **564**, 914 (2002).
[44] K. Mori, J. C. Chonko, and C. J. Hailey, Astrophys. J. **631**, 1082 (2005).
[45] K. Mori and C. J. Hailey, Astrophys. J. **648**, 1139 (2006).
[46] W. C. G. Ho, D. Lai, A. Y. Potekhin, and G. Chabrier, Adv. Space Res. **33**, 537 (2004).
[47] P. J. Reynolds, D. M. Ceperley, B. J. Alder, and W. A. Lester, Jr., J. Chem. Phys. **77**, 5593 (1982).
[48] D. M. Ceperley and B. Bernu, J. Chem. Phys. **89**, 6316 (1988).
[49] N. Metropolis, A. W. Rosenbluth, M. N. Rosenbluth, A. H. Teller, and E. Teller, J. Chem. Phys. **21**, 1087 (1953).
[50] B. L. Hammond, W. A. Lester, Jr., and P. J. Reynolds, *Monte Carlo Methods in Ab Initio Quantum Chemistry* (World Scientific, Singapore, 1994).
[51] G. Ortiz, D. M. Ceperley, and R. M. Martin, Phys. Rev. Lett. **71**, 2777 (1993).
[52] M. D. Jones, G. Ortiz, and D. M. Ceperley, Phys. Rev. E **55**, 6202 (1997).
[53] L. I. Schiff and H. Snyder, Phys. Rev. **55**, 59 (1937).
[54] M. Klews, Ph.D. thesis, University of Tübingen, 2003, http://tobias-lib.ub.uni-tuebingen.de/volltexte/ 2003/1022/
[55] C. de Boor, SIAM (Soc. Ind. Appl. Math.) J. Numer. Anal. **14**, 441 (1977).
[56] C. de Boor, *A Practical Guide to Splines* (Springer, Heidelberg, 1978).
[57] D. Engel, M. Klews, and G. Wunner (unpublished).
[58] T. Kato, Commun. Pure Appl. Math. **10**, 151 (1957).
[59] V. G. Bezchastnov, G. G. Pavlov, and J. Ventura, Phys. Rev. A **58**, 180 (1998).